

Electron production by solar Ly- α line radiation in the ionospheric D-region

Aleksandra Nina^{a,*}, Vladimir M. Čadež^b

^a*Institute of Physics, University of Belgrade, Pregrevica 118, Belgrade, Serbia*

^b*Astronomical Observatory, Volgina 7, 11060 Belgrade, Serbia*

Abstract

The hydrogen Ly- α line has a dominant influence in photo-ionization processes in the unperturbed terrestrial ionospheric D region. In this paper, we present a procedure of calculating the rate of photo-ionization induced by Ly- α photons based on relaxation of electron density after intensive perturbations like those caused by solar X flares. This theory is applied to the ends of relaxation periods following three cases of solar X flares from May 5, 2010, February 18, 2011 and March 24, 2011. The necessary data on low ionospheric plasma parameters were collected by the very low frequency (VLF) radio-wave technics. The electron concentration is calculated from the amplitude and phase of the VLF signal emitted by the DHO transmitter in Germany and recorded by a receiver located in Serbia.

Keywords: solar Ly- α line; solar X-flare; ionospheric D region; photo-ionization

1. Introduction

As a part of terrestrial atmosphere, the ionosphere is under permanent variable influences coming from outer space and Earth's atmosphere and lithosphere. The non-periodic and sudden events, such as solar flares (McRae and Thomson, 2004; Nina et al., 2012a, 2011; Kolarski et al., 2011), coronal mass ejections (Balan et al., 2008; Bochev and Dimitrova, 2003), influences of the processes in remote parts of the universe like supernova explosions followed by hard X and γ radiation (Inan et al., 2007), lightnings (Voss et al., 1998; Collier et al., 2011), and some processes in the Earth lithosphere like volcanic eruptions and earthquakes (Utada et al., 2011; Heki and Ping, 2005) temporarily induce space and time changeable ionospheric perturbations. The variability of affects caused by permanent sources of perturbations, like the quiet Sun radiation or cosmic rays, lies in variations of their initial intensity, of attenuation during propagation to the considered location and, finally, of the total cross-section for the analyzed process. In addition to a purely scientific interest, studying the effects of specific ionospheric plasma perturbers finds practical applications, primarily in telecommunications. Namely, changes in the signal characteristics caused by varying ionospheric plasma conditions and compositions, require their predictions in order to deal with disturbances in signal reception.

One of the most important external influences on the chemical processes in the lowest ionospheric layer, called the D region, is coming from the solar Ly- α line (121.6 nm) radiation whose presence is periodically intensified during

the day. Generally, in local plasma this line participates in several processes such as the oxygen and water cluster dissociation, and chemistry of minor species such as water vapor, ozone and nitric oxide (Woods et al., 2000). In this paper we are interested in production of electrons in plasma located in the middle part of the D region as a result of NO molecule photo-ionization by Ly- α photons. A very important significance of this process lies in the fact that the formation of the D region in the daytime is primarily a result of the photo-ionization by Ly- α photons (Nicolet and Aikin, 1960), and reversly, reduction of the incoming solar flux including the Ly- α line is followed by disappearance of the lowest ionospheric layer during the nighttime conditions. The rate of this process depends on the incident Ly- α flux, its attenuation during propagation though higher atmospheric layers and on the NO density in local plasma. As numerous studies have shown, all these parameters are variable in space and time and they can be calculated from experimental data obtained by various observational technics.

Data sets for the Ly- α irradiance are modeled based on values recorded by satellites such as, for example, the Atmospheric Explorer E (AE-E), the Solar Mesospheric Explorer (SME), and the Upper Atmosphere Research Satellite (UARS), and variations in the Ly- α irradiance during solar cycles and seasons are presented in Woods et al. (2000); Fröhlich (2009); Correia et al. (2011).

The atmospheric Ly- α line absorption coefficients can be obtained from data gathered by rockets, balloons, space shuttle and satellite measurements, and the results exhibit a strong zenith angle dependency which is analyzed in Kockarts (2002). Also, measurements of the NO density show values within a wide range at fixed altitudes (Aikin et al. (1964); Pearce (1969); Barabash et al. (2012) and

*Corresponding author

Email addresses: sandrast@ipb.ac.rs (Aleksandra Nina), vcadez@aob.rs (Vladimir M. Čadež)

references therein). As the incident flux of the Ly- α line, its absorption coefficient, and the NO density at considered altitudes may have different values, the resulting rate of relevant photo-ionization process varies within 3 order of magnitudes (Aikin, 1969).

In this work, we present a new procedure for determining the photo-ionization rate induced by the Ly- α line in the middle parts of the D region at altitudes between around 70 and 80 km during the relaxation period after larger perturbations such as solar flares. The basic points of our approach are based on occurrence of transient ionospheric perturbations resulting in electron density change and the fact that the perturbed plasma tends to the original state once the action of the perturber is over.

Generally, there are several global models that can be used to determine the electron density in the D region such as the International Reference Ionosphere (IRI) model (Bilitza, 1992) (an empirical model of unperturbed ionosphere that can be applied to the altitude range between 50 and 2000 km and that use rocket measurements as data base to determine the electron density in the D region), the Sodankyla Ion Chemistry (SIC) model (Turunen et al., 1992) (it was built to be a tool for interpretation of D-region incoherent scatter experiments and cosmic radio-noise absorption measurements and it can be run either as a steady-state model or a time-dependent model) and Mitra-Rowe chemical model (Mitra and Rowe, 1972) in which electron density can be calculated by adjusting free parameters according to rocket-borne mass spectrometer measurements.

The suggested new theoretical procedure utilizes data that can be obtained by a continuous monitoring of the low ionosphere using primarily ground based technics: the radar and very low frequency (VLF) radio signal measurements. The advantage of the latter is seen in numerous transmitters and receivers located worldwide, which provides a possibility to analyze a large part of the low ionosphere. The theoretical equations are applied to examples of low ionospheric perturbation taking three solar X flares as a convenient perturbing mechanism. The electron density time and altitude dependencies are calculated from data obtained by the D region monitoring using VLF radio signals emitted by the DHO transmitter located in Germany and recorded in Serbia by the AWESOME (Atmospheric Weather Electromagnetic System for Observation Modeling and Education) receiver (Scherrer et al., 2008) within the Stanford/AWESOME Collaboration for Global VLF Research activities.

2. Theoretical backgrounds

Unlike the existing procedures for determining the Ly- α photo-ionization rate in the ionosphere from calculated data related to the Ly- α radiation entering the terrestrial atmosphere, its attenuation during propagation in the gas, and the NO density at locations of interest, in this work we present a method that requires knowledge of the electron

density time variations in the studied local medium in the aftermath of an intensive perturbation when variations in ionization rate are not large. This excludes periods of the local sunrise and sunset, and time intervals characterized by large variations in photons and/or particle radiation in the domain of sufficiently large energies to ionize some of species in the low ionospheric plasma.

As in the case of many similar studies like Mitra (1974) and McEwan and Phillips (1978), we start from the general form of the electron density dynamic:

$$\frac{dN(\vec{r}, t)}{dt} = \mathcal{G}(\vec{r}, t) - \mathcal{L}(\vec{r}, t), \quad (1)$$

where $N(\vec{r}, t)$, $\mathcal{G}(\vec{r}, t)$ and $\mathcal{L}(\vec{r}, t)$ are electron density, electron gain and electron loss rates, respectively at location \vec{r} and at time t . Here, the influence of transport processes is neglected as they become important at altitudes above 120-150 km (Blaunstein and Christodoulou, 2006) and they are generally not included in models of the D region plasma (Turunen et al., 1992; William and Foley, 1978). The above Eq. (1) is very complicated in its general form due to complexity of terms $\mathcal{G}(\vec{r}, t)$ and $\mathcal{L}(\vec{r}, t)$. For this reason, they can first be expressed in a form composed of quantities whose values can be obtained from observations and from modeling, which allows for calculations of the photo-ionization rate induced by the Ly- α line. In the case of absence of intensive sudden influences coming from the Earth, the dominant D region plasma ionization is caused by perturbers from the outer space.

The contribution of these photons and particles on the low ionospheric plasma processes depends on their fluxes entering the atmosphere, attenuations during the propagation through higher atmospheric layers, and on the total ionization cross section at considered location. As to the photo-ionization, the required wavelengths for the D region main species N_2 , O_2 , NO, and O are less than 79.6, 102.7, 134.0, and 91.1 nm, respectively, and $102.7 \text{ nm} \leq \lambda \leq 111.8 \text{ nm}$ for the metastable $O_2(^1\Delta_g)$. The variability of the electron production in the D layer thus depends on the type and intensity of the incoming radiation. For example, the hard X and gamma radiation penetrates the atmosphere with comparatively lower attenuation but their photo-ionization cross sections for the involved plasma constituents are much smaller than for other photons with smaller energy (Berger et al., 1998). Contrary, the large part of the UV domain has a strong attenuation in the higher atmospheric layers above the D region (Ratcliffe, 1972). Consequently, typical moderate intensity variations of these two types of radiation have little influence on the electron production in the D region. In the case without sudden perturbations, the published investigations (for example McEwan and Phillips (1978); Thomas (1974) and references therein) show that Ly- α , cosmic, and the radiation at wavelength domain between 102.7 and 111.8 nm (these photons can ionize the metastable molecule $O_2(^1\Delta_g)$) can be considered the main ionization sources. However, these studies show that the

ionization rate induced by cosmic rays decreases with altitude and its influence can be negligible above about 70 km. Finally, the influence of radiation between 102.7 and 111.8 nm is smaller than that of Ly- α photons at altitudes h between 70 and 80 km. Consequently, we can assume that the $\mathcal{G}(\vec{r})$ is approximately equal to the photo-ionization rate induced in the D region by the $\mathcal{G}_{Ly\alpha}(\vec{r})$ radiation at considered heights:

$$\mathcal{G}(\vec{r}) = \mathcal{G}_{Ly\alpha}(\vec{r}), \quad 70\text{km} \leq h \leq 80\text{km}. \quad (2)$$

Here, we assumed that time variation of the ionization rate is not significant and we can ignore the variable t .

There are many processes in the ionosphere that result into electron density reduction. The rates of these processes depend on the structure and state of plasma in the considered medium in time and space. The recombination processes including the electron-ion, ion-ion and three body recombination have very important role so that the electron loss rate can be expressed as (Mitra, 1974; Žigman et al., 2007):

$$\mathcal{L}(\vec{r}, t) = \xi_L(\vec{r}, t)N^2(\vec{r}, t), \quad (3)$$

where $\xi_L(\vec{r}, t)$ is the effective recombination coefficient.

Finally, the Eqs (1) and (3) give:

$$\frac{dN(\vec{r}, t)}{dt} = \mathcal{G}(\vec{r}, t) - \xi_L(\vec{r}, t)N^2(\vec{r}, t). \quad (4)$$

The quantities in Eq. (4) can be determined by combining the observational data, numerical modeling, and theoretical procedure. In this sense, the electron density and its time derivative can be calculated indirectly from numerically processed data recorded by different technics like the radar and VLF radio signal monitoring of the low ionosphere while the electron gain rate $\mathcal{G}(\vec{r}, t)$ and coefficient $\xi_L(\vec{r}, t)$ will be determined by the theoretical procedure that follows.

In Eq. (2), the Ly- α photo-ionization rate $\mathcal{G}_{Ly\alpha}(\vec{r})$ which is related to conditionally unperturbed ionosphere, can be derived from Eq. (4) applied to the late stage of perturbation relaxation in the aftermath of the flare. Thus, it is not necessary to know values of parameters in Eq. (4) during the entire flare period and the analysis can be restricted to the late stage of plasma relaxation to the initial state provided the large fluctuation due to Ly-alpha emission, and possible other perturbations like particle and electromagnetic (continuum and spectral lines radiation) are absent. In this case, the variations of $\mathcal{G}(\vec{r}, t)$ and $\xi_L(\vec{r}, t)$ become weakly time dependent and we assume them approximately constant within some finite time interval Δt :

$$\begin{aligned} \mathcal{G}(\vec{r}, t - \Delta t) &\approx \mathcal{G}(\vec{r}, t) \equiv \bar{\mathcal{G}}(\vec{r}, t), \\ \xi_L(\vec{r}, t - \Delta t) &\approx \xi_L(\vec{r}, t) \equiv \bar{\xi}_L(\vec{r}, t). \end{aligned}$$

Eq. (4) can now be applied to the interval end points $t_1 = t - \Delta t$ and $t_2 = t$ which yields the following set of

two algebraic equations for the unknown quantities $\bar{\mathcal{G}}(\vec{r}, t)$ and $\bar{\xi}_L(\vec{r}, t)$:

$$\begin{aligned} \left. \frac{dN}{dt} \right|_{\vec{r}, t - \Delta t} &= \bar{\mathcal{G}}(\vec{r}, t) - \bar{\xi}_L(\vec{r}, t)N^2(\vec{r}, t - \Delta t) \\ \left. \frac{dN}{dt} \right|_{\vec{r}, t} &= \bar{\mathcal{G}}(\vec{r}, t) - \bar{\xi}_L(\vec{r}, t)N^2(\vec{r}, t) \end{aligned} \quad (5)$$

which finally yields the expression for $\bar{\mathcal{G}}(\vec{r}, t)$:

$$\mathcal{G}(\vec{r}, t) = \frac{N^2(\vec{r}, t) \left. \frac{dN}{dt} \right|_{\vec{r}, t - \Delta t} - N^2(\vec{r}, t - \Delta t) \left. \frac{dN}{dt} \right|_{\vec{r}, t}}{N^2(\vec{r}, t) - N^2(\vec{r}, t - \Delta t)}. \quad (6)$$

The above analysis thus allows estimates of $\mathcal{G}_{Ly\alpha}(\vec{r})$ through expressions Eq. (2) and Eq. (6). Here we wish to point out that the length of the relaxation period has to be large enough for the described procedure to be performed. As, on the other hand, this length depends on the intensity of the initial ionospheric perturbation, it means that only sufficiently intensive ionospheric perturbations (like solar flares class C or stronger) can be treated by our analysis.

3. Electron density modeling

As in the case of numerous papers (McRae and Thomson, 2000; Grubor et al., 2008; Žigman et al., 2007; Thomson et al., 2011; Nina et al., 2011, 2012a,b), our calculation of electron density is based on the observed VLF signal data and their comparison with data obtained by simulations of the VLF signal propagation using the Long-Wave Propagation Capability (LWPC) numerical code (developed by the Naval Ocean Systems Center (NOSC), San Diego, USA (Ferguson, 1998)). This numerical code uses Wait's model of vertically stratified ionosphere (Wait and Spies, 1964) characterized by two independent parameters, the signal reflection height $H'(t)$ and sharpness $\beta(t)$ (related to the electron density gradient as shown in Nina et al. (2012a)) which yields the following analytical expression for the electron density $N(h, t)$:

$$N(h, t) = 1.43 \cdot 10^{13} e^{-\beta(t)H'(t)} e^{(\beta(t)-0.15)h}. \quad (7)$$

Here, it should be noted that the application of this method to calculate the electron density assumes the spatial dependence of the quantities in Eq. (6) be reduced only to altitude h according to the approximation of the low ionosphere stratification. Consequently, the forthcoming analysis requires data for signals that propagate through a medium whose plasma characteristics do not vary, at least locally, in the horizontal plane. This has to be taken into account i.e. signals from VLF transmitters located not too far from the receiver should be chosen in the analysis.

In the Eq. 7, both parameters $H'(t)$ and $\beta(t)$ are time dependent even if sudden ionospheric disturbances are absent. This, namely, comes from long time-dependent phe-

nomena in the D-region like periodic variations in atmospheric composition, diurnal and seasonal variations of ionizing radiation intensity due to changes of solar zenith angle, and variations of radiation related to the solar cycle phase. The dependence of $H'(t)$ and $\beta(t)$ on geographical position due to different local solar zenith angles is calculated in literature for different periods of the solar cycle by, for example, detections of VLF radio atmospheric through VLF broadband observations (Han et al., 2011), and by comparisons of narrowband VLF data with simulations of signal propagation utilizing numerical codes such as LWPC (Thomson, 1993; McRae and Thomson, 2000). Because of numerous influences affecting the D region plasma, the parameters $H'(t)$ and $\beta(t)$ are shown to fall within intervals 70-75 km and $0.2-0.5 \text{ km}^{-1}$ during daytime in the case of quiet ionosphere (Ferguson, 1998).

In addition to differences in physical and chemical conditions explained above, the obtained discrepancies in calculated values result from application of different models like IRI (Bilitza, 1992) and FIRI (Friedrich and Torkar, 2001). In calculations that include solar zenith dependence of Wait's parameters, the discrepancies among obtained $H'(t)$ and $\beta(t)$ are more pronounced at higher zenith angles. On the other hand, for smaller solar zenith angles, the time and space variations of plasma parameters are not so large and we can assume $H'(t)$, $\beta(t) \approx \text{const}$ for signals propagating along paths for which the solar zenith angle does not change much, and when the observation time is sufficiently short. This assumption of quasi constancy of β and H' will be applied in treatment that follows.

4. Observed data and experimental setup

We study the time period of ionospheric relaxation in the aftermath of perturbations induced by three solar X flares occurred on May 5th, 2010 (Case I), February 18th, 2011 (Case II) and March 24th, 2011 (Case III) whose impacts on Earth's atmosphere are registered by satellites GOES-14 (Fig. 1, top panel, Case I) and GOES-15 (Fig. 1, middle and bottom panels, Case II and III)

To calculate altitude and time dependencies of the electron density $N(h, t)$, we perform the ground based low ionosphere monitoring using the 23.4 kHz VLF radio signal emitted by the DHO transmitter in Rhauderfehn (Germany) and recorded by the AWESOME VLF receiver located in Institute of Physics in Belgrade (Serbia). This transmitter was chosen because it provides the best quality of the recorded signal owing to the high emission power of 800 kW and suitable signal frequency for the location of the receiver, and a relatively short signal propagation path. The latter property is important as it excludes significant variations in vertical stratification of parameters in the ambient ionospheric plasma. The amplitude and phase time variations of the recorded signal during the low ionosphere responses to the considered perturbing flares are shown in the Fig. 1 and their role in electron density calculations are explained in the next section.

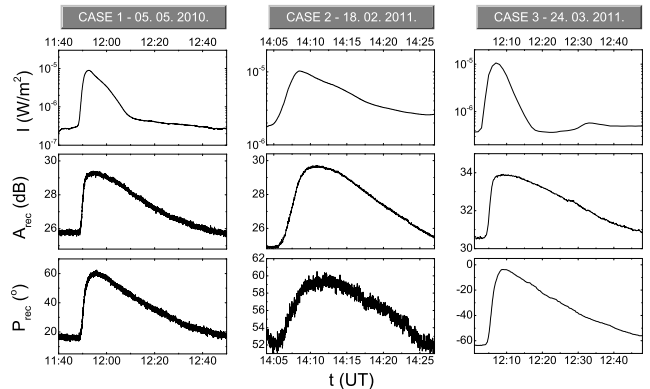


Figure 1: Time dependencies of the intensity of X radiation registered by satellites in the wavelength domain between 0.1 and 0.8 nm (top panels), and signal amplitude (middle panels) and phase (bottom panels) registered by AWESOME receiver located in Belgrade (Serbia) during presence three solar flares occurred on May 5th, 2010 (Case I), February 18th, 2011 (Case II), and March 24th, 2011 (Case III).

As we can see from Fig. 1 the intensities of X-radiation decrease in time at the final part of the indicated time periods and they reach values existing prior to flare events. Within the same time period, the signal data show monotonous relaxations without visible additional changes. In the section that follows, it will be shown that zenith angles along the trajectory are small and do not change significantly during the observed time interval for the three considered cases. All these facts together allow us to apply the presented theoretical model to studied cases.

5. Results

As can be seen from Eq. 6, for the electron gain rate $\mathcal{G}(h, t)$ that tends to $\mathcal{G}_{Ly\alpha}(h)$ according to Eq. (2), it is first necessary to determine the altitude and time dependencies of electron density $N(h, t)$. In this work, in calculations we consider a relatively short observational period (around 30 s) and relatively short path of VLF signals characterized by small differences in solar zenith angle between locations of the transmitter (latitude 53.1 N and longitude 7.6 E) and the receiver (latitude 44.8 N and longitude 20.4 E) which are: 40.5 and 40.3, 54.0 and 51.4, and 66.4 and 62.4 for the Case I, Case II and Case III, respectively. The calculation given in Han et al. (2011), McRae and Thomson (2000) and Friedrich and Torkar (2001) for considered angles predict very small differences in parameters which yields small electron density changes. The relevant values are given in Table 2 where data obtained by foregoing methods are considered separately. Here, we can see that along the trajectory the maximum deviations from the mean values relevant for the geographic locations of the transmitter and the receiver are very small, less than about 1% for β , 2% for H' and 20% for N_e . This allows us

to assume constant parameters in the unperturbed ionosphere which are then referent values for determined time dependencies of parameters during perturbations. Here, we present calculation that includes constant values $\beta = 0.3 \text{ km}^{-1}$ for sharpness and $H' = 74 \text{ km}$ for the reflection height in unperturbed plasma, also used in previous works (Žigman et al., 2007; Grubor et al., 2008; Nina et al., 2011, 2012a,b). These chosen values lie within presented relevant data for all considered angles.

The time distributions of obtained parameters $H'(t)$ and $\beta(t)$ and electron density $N(h, t)$ at different heights during the entire period of ionospheric response to the solar X flare are presented in Figs 2 and 3.

The obtained values of parameters $H'(t_{I_{max}})$ and $\beta(t_{I_{max}})$, and the electron densities $N(h, t_{I_{max}})$ at flare intensity peaks are in a good agreement with values presented in Grubor et al. (2008), Thomson et al. (2005) and Žigman et al. (2007).

To calculate the electron density time derivative, we a suitable fitting function for the electron density time dependence in the relaxation period. We thus eliminate small (in our analysis) non important variations in $N(h, t)$ caused by other perturbers and consider only the general time tendencies. The fitted curves are shown in Fig. 3 by solid lines, and the calculated time variations of the electron density time derivative are presented in the Fig. 4 where we can see that these time derivatives are negative and, after sufficiently long time, they approach zero at all considered altitudes. These two facts practically indicate the return of plasma to its initial state.

Generally, the very slow variation of plasma characteristics at the end of considered time periods as seen, in Figs 1-4, enables the application of the presented theoretical model in the indicated time intervals and calculations of time dependencies of $\mathcal{G}(h, t)$ presented in Fig. 5 for heights 70, 75 and 80 km. Here, we can see that electron gain rates are practically time independent and we can assume that these values approximately determine the electron gain rates $\mathcal{G}_{Ly\alpha}(h)$ induced by the Ly- α line.

The altitude distribution of $\mathcal{G}(h, t)$ can be found from Wait's equation for electron density Eq. (7). Namely, it yields the following ratio of electron densities $N(h_1, t)$ and $N(h_2, t)$ at heights h_1 and h_2 , respectively:

$$\frac{N(t, h_1)}{N(t, h_2)} = e^{(\beta(t)-0.15)(h_1-h_2)}. \quad (8)$$

If we further consider the ratio of the ionization rates at these altitudes, $\mathcal{G}(t, h_1)$ and $\mathcal{G}(t, h_2)$, and taking into account that $\beta(t)$ is practically constant at the ends of considered time intervals, Eqs (6) and (8) give:

$$\frac{\mathcal{G}(t, h_1)}{\mathcal{G}(t, h_2)} \approx e^{(\beta(t)-0.15)(h_1-h_2)}. \quad (9)$$

The obtained values for $\mathcal{G}_{Ly\alpha}(75\text{km})$ and $\beta(t)$ at the ends of the considered time intervals are inserted into the Eq. (10) which yields the altitude distributions of the electron gain

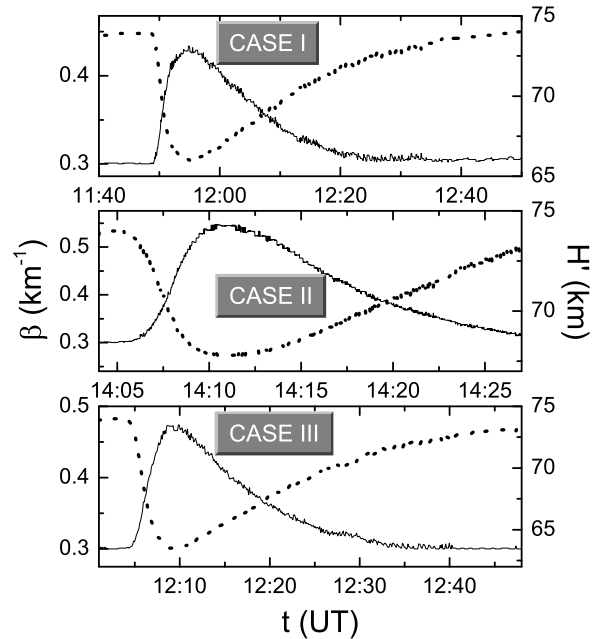


Figure 2: Time dependencies of Wait's parameters during the considered flare activities. Solid and dotted lines are related to sharpness $\beta(t)$ and signal reflection height $H'(t)$, respectively.

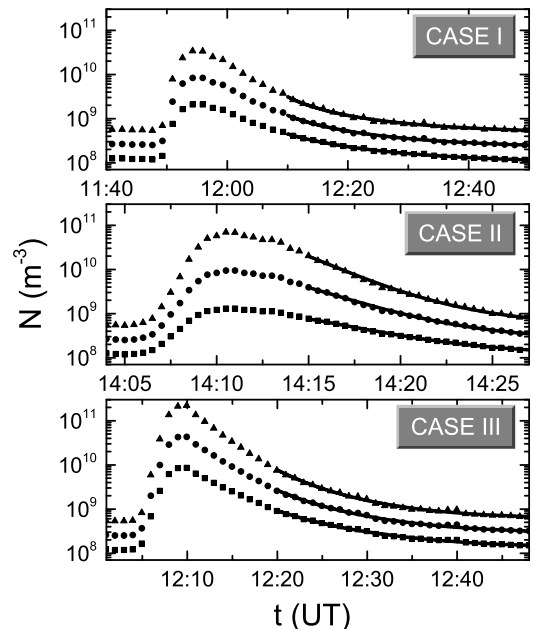


Figure 3: Time dependencies of the electron density at altitudes 70 km (squares), 75 km (circles) and 80 km (triangles) during the considered flare activities.

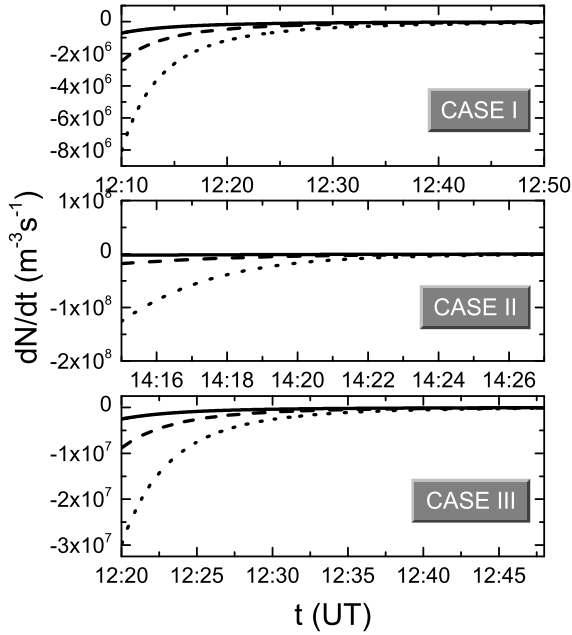


Figure 4: Time dependencies of the electron density time derivative at altitudes 70 km (solid lines), 75 km (dashed lines) and 80 km (dotted lines) during relaxation periods.

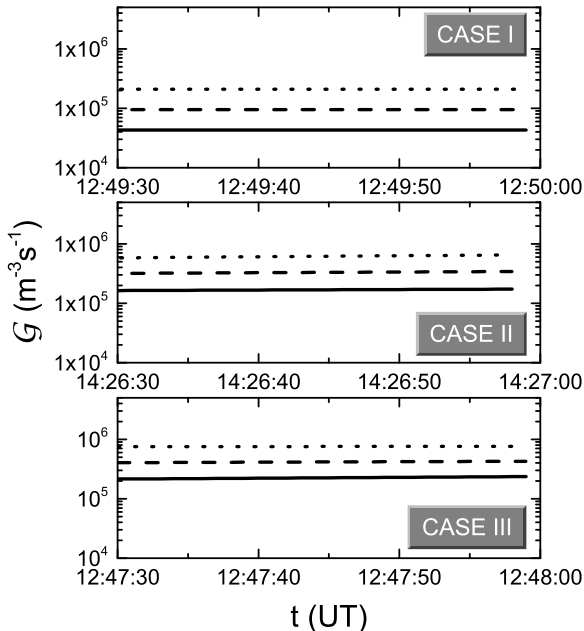


Figure 5: Time dependencies of the electron gain rate $\mathcal{G}(h, t)$ at altitudes 70 km (solid lines), 75 km (dashed lines) and 80 km (dotted lines) during the periods relevant to applying method.

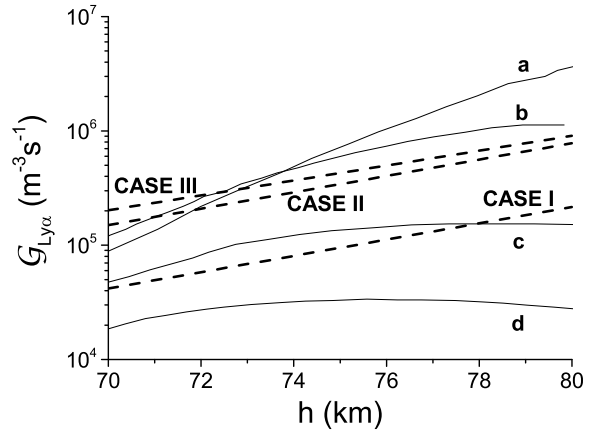


Figure 6: Altitude dependencies of the electron gain rate $\mathcal{G}_{Ly\alpha}(h)$ for Case I, II and III, and their comparison with data presented in Mitra (1977) (a), Rowe (1972) (b), Aikin et al. (1964) (c) and Bourdeau et al. (1965) (d).

rate induced by the Ly- α line as shown in Fig. 6. Here, we can see that our model, when applied to the low ionospheric plasma perturbations induced by considered flares, gives the Ly- α photo-ionization rates that fall within the domain of values presented in Mitra (1977); Rowe (1972); Aikin et al. (1964) and Bourdeau et al. (1965). As we said in Introduction, the differences in the presented altitude variations are due to different plasma and propagation conditions, and due to different Ly- α intensities.

The error factor of our method, EF , defined as the ratio of $\mathcal{G}'_{Ly\alpha}(h)$ to $\mathcal{G}_{Ly\alpha}(h)$, where values of $\mathcal{G}'_{Ly\alpha}(h)$ are calculated from electron densities obtained by methods taking into account the Wait's parameters dependencies of the solar zenith angle, can be obtained from Eq. (6) as:

$$EF \equiv \frac{\mathcal{G}'_{Ly\alpha}(h)}{\mathcal{G}_{Ly\alpha}(h)} \approx \frac{N'(h)}{N(h)}. \quad (10)$$

We take here the electron density ratio obtained by two methods to be practically constant, i.e. $N'(h, t)/N(h, t) \approx const.$ This approximation is justified because of very small changes in plasma parameters within considered short time period. Table 2 shows comparisons of EF obtained by our method with those given in Han et al. (2011), McRae and Thomson (2000) and Friedrich and Torkar (2001). Taking into account spreads of results shown in Fig. 6 where the presented values differ by three orders of magnitude, we can conclude that our calculated error factor ($EF < 4$ in all three considered cases) can be taken as relatively very small. From this fact and from comparisons with existing data shown in Fig. 6, we conclude that the presented calculating procedure of the photo-ionization rate induced by the Ly- α line radiation gives values which do not significantly depend on the method how the electron density is calculated, and which are consistent with values from the literature.

6. Summary

In this paper, we present a new theoretical procedure for calculations of the photo-ionization rate in the terrestrial ionospheric D region induced by the Ly- α line radiation coming from the Sun. This method is based on a slow time variation of plasma characteristics during the relaxation period following a large perturbation like that caused by a solar X flare. It requires observational data to determine the electron density at the considered location, which can be obtained from the D region monitoring.

The theoretical results are applied to three cases with solar X flares occurred on May 5th, 2010, February 18, 2011 and March 24, 2011, where we used the amplitude and phase time variations of the VLF radio signal emitted by the DHO transmitter in Germany and recorded by the AWESOME receiver located in Serbia for low ionosphere monitoring. The obtained altitude distributions of the photo-ionization rate (order of magnitudes 10^4 to 10^5 m⁻³s⁻¹) are in a good agreement with data existing in the literature.

Acknowledgments

The present work was supported by the Ministry of Education, Science and Technological Development of the Republic of Serbia as a part of the projects no. III 44002, 176002 and 176004.

References

- Aikin, A. C., 1969. The Ion Pair Production Function of the Lower Ionosphere, National Aeronautics and Space Administration. Goddard Space Flight Center, Greenbelt, Md.
- Aikin, A. C., Kane, J. A., Troim, J., Nov. 1964. Some Results of Rocket Experiments in the Quiet D Region. *J. Geophys. Res.* 69, 4621–4628.
- Balan, N., Alleyne, H., Walker, S., Reme, H., McCrea, I., Aylward, A., Dec. 2008. Magnetosphere-ionosphere coupling during the CME events of 07-12 November 2004. *J. Atmos. Sol.-Terr. Phys.* 70, 2101–2111.
- Barabash, V., Osepian, A., Dalin, P., Kirkwood, S., Sep. 2012. Electron density profiles in the quiet lower ionosphere based on the results of modeling and experimental data. *Ann. Geophys.* 30, 1345–1360.
- Berger, M. J., Hubbell, J. H., Seltzer, S. M., Chang, J., Coursey, J. S., Sukumar, R., Zucker, D. S., 1998. XCOM: Photon Cross Sections Database. <http://physics.nist.gov/PhysRefData/Xcom/Text/XCOM.html>.
- Bilitza, D., Apr. 1992. International reference ionosphere (1990). *Planet. Space. Sci.* 40, 544–544.
- Blaunstein, N., Christodoulou, C., 2006. Radio Propagation and Adaptive Antennas for Wireless Communication Links: Terrestrial, Atmospheric and Ionospheric, John Wiley and Sons, Inc. Hoboken, New Jersey.
- Bochev, A. Z., Dimitrova, I. I. A., 2003. Magnetic cloud and magnetosphere - ionosphere response to the 6 November 1997 CME. *Adv. Space. Res.* 32, 1981–1987.
- Bourdeau, R. E., Aiken, A. C., Donley, J. L., 1965. The Lower Ionosphere at Solar Minimum, Greenbelt, Md.: NASA, Goddard Space Flight Center.
- Collier, A. B., Lichtenberger, J., Clilverd, M. A., Rodger, C. J., Steinbach, P., Mar. 2011. Source region for whistlers detected at Rothera, Antarctica. *J. Geophys. Res.* 116, 3219–3231.
- Correia, E., Kaufmann, P., Raulin, J.-P., Bertoni, F., Gavilan, H. R., Oct. 2011. Analysis of daytime ionosphere behavior between 2004 and 2008 in Antarctica. *J. Atmos. Sol.-Terr. Phys.* 73, 2272–2278.
- Ferguson, J. A., 1998. Computer Programs for Assessment of Long-Wavelength Radio Communications, Version 2.0, Technical document 3030, Space and Naval Warfare Systems Center, San Diego CA .
- Friedrich, M., Torkar, K. M., Oct. 2001. FIRI: A semiempirical model of the lower ionosphere. *J. Geophys. Res.* 106, 21409–21418.
- Fröhlich, C., Jul. 2009. Evidence of a long-term trend in total solar irradiance. *Astron. Astrophys.* 501, L27–L30.
- Grubor, D. P., Šulić, D. M., Žigman, V., Jun. 2008. Classification of X-ray solar flares regarding their effects on the lower ionosphere electron density profile. *Ann. Geophys.* 26, 1731–1740.
- Han, F., Cummer, S. A., Li, J., Lu, G., May 2011. Daytime ionospheric D region sharpness derived from VLF radio atmospherics. *J. Geophys. Res.* 116, 5314–5324.
- Heki, K., Ping, J., Aug. 2005. Directivity and apparent velocity of the coseismic ionospheric disturbances observed with a dense GPS array. *Earth. Planet. Sc. Lett.* 236, 845–855.
- Inan, U. S., Lehtinen, N. G., Moore, R. C., Hurley, K., Boggs, S., Smith, D. M., Fishman, G. J., Apr. 2007. Massive disturbance of the daytime lower ionosphere by the giant γ -ray flare from magnetar SGR 1806-20. *Geophys. Res. Lett.* 34, 8103–8108.
- Kockarts, G., May 2002. Aeronomy, a 20th Century emergent science: the role of solar Lyman series. *Ann. Geophys.* 20, 585–598.
- Kolarski, A., Grubor, D., Šulić, D., 2011. Diagnostics of the Solar X-Flare Impact on Lower Ionosphere through Seasons Based on VLF-NAA Signal Recordings. *Balt. Astron.* 20, 591–595.
- McEwan, M., Phillips, F., 1978. Chemistry of the Atmosphere, Mir, Moscow.
- McRae, W. M., Thomson, N. R., May 2000. VLF phase and amplitude: daytime ionospheric parameters. *J. Atmos. Sol.-Terr. Phys.* 62, 609–618.
- McRae, W. M., Thomson, N. R., Jan. 2004. Solar flare induced ionospheric D-region enhancements from VLF phase and amplitude observations. *J. Atmos. Sol.-Terr. Phys.* 66, 77–87.
- Mitra, A. P. (Ed.), 1974. Ionospheric effects of solar flares. Vol. 46 of Astrophysics and Space Science Library, D. Reidel Publishing Company, Boston.
- Mitra, A. P., 1977. Ionospheric Effects of Solar Flares, Mir, Moscow.
- Mitra, A. P., Rowe, J. N., May 1972. Ionospheric effects of solar flares - VI. Changes in D-region ion chemistry during solar flares. *J. Atmos. Sol.-Terr. Phys.* 34, 795–806.
- Nicolet, M., Aikin, A. C., May 1960. The Formation of the D Region of the Ionosphere. *J. Geophys. Res.* 65, 1469–1483.
- Nina, A., Čadež, V., Srećković, V., Šulić, D., May 2012a. Altitude distribution of electron concentration in ionospheric D-region in presence of time-varying solar radiation flux. *Nucl. Instrum. Meth. B* 279, 110–113.
- Nina, A., Čadež, V., Srećković, V. A., Šulić, D., 2011. The Influence of Solar Spectral Lines on Electron Concentration in Terrestrial Ionosphere. *Balt. Astron.* 20, 609–612.
- Nina, A., Čadež, V., Šulić, D., Srećković, V., Žigman, V., May 2012b. Effective electron recombination coefficient in ionospheric D-region during the relaxation regime after solar flare from February 18, 2011. *Nucl. Instrum. Meth. B* 279, 106–109.
- Pearce, J. B., 1969. Rocket measurement of nitric oxide between 60 and 96 kilometers. *J. Geophys. Res.* 74, 853–861.
- Ratcliffe, J. A., 1972. An Introduction to the Ionosphere and the Magnetosphere, Cambridge University Press, Cambridge.
- Rowe, J. N., 1972. Model studies of the lower ionosphere, Sci. Rep.No. 406, Pennsylvania State Univ., Univ. Park, USA.
- Scherrer, D., Cohen, M., Hoeksema, T., Inan, U., Mitchell, R., Scherrer, P., Dec. 2008. Distributing space weather monitoring instruments and educational materials worldwide for IHY 2007: The AWESOME and SID project. *Adv. Space. Res.* 42, 1777–1785.
- Thomas, L., Feb. 1974. Recent developments and outstanding problems in the theory of the D region. *Radio Sci.* 9, 121–136.
- Thomson, N. R., Feb. 1993. Experimental daytime VLF ionospheric parameters. *J. Atmos. Sol.-Terr. Phys.* 55, 173–184.

- Thomson, N. R., Rodger, C. J., Clilverd, M. A., Jun. 2005. Large solar flares and their ionospheric D region enhancements. *J. Geophys. Res. (Space Physics)* 110, 6306-6315.
- Thomson, N. R., Rodger, C. J., Clilverd, M. A., Nov. 2011. Daytime D region parameters from long-path VLF phase and amplitude. *J. Geophys. Res.* 116, 11305-11310.
- Turunen, E., Tolvanen, J., Matveinen, H., Ranta, H., 1992. D Region Ion Chemistry Model, in STEP Handbook of Ionospheric Models, R. W. Schunk, Boulder, Colorado, USA.
- Utada, H., Shimizu, H., Ogawa, T., Maeda, T., Furumura, T., Yamamoto, T., Yamazaki, N., Yoshitake, Y., Nagamachi, S., Nov. 2011. Geomagnetic field changes in response to the 2011 off the Pacific Coast of Tohoku Earthquake and Tsunami. *Earth. Planet. Sc. Lett.* 311, 11-27.
- Žigman, V., Grubor, D., Šulić, D., May 2007. D-region electron density evaluated from VLF amplitude time delay during X-ray solar flares. *J. Atmos. Sol.-Terr. Phy.* 69, 775-792.
- Voss, H. D., Walt, M., Imhof, W. L., Mobilia, J., Inan, U. S., Jun. 1998. Satellite observations of lightning-induced electron precipitation. *J. Geophys. Res.* 103, 11725-11744.
- Wait, J. R., Spies, K. P., 1964. Characteristics of the Earth-ionosphere waveguide for VLF radio waves, NBS Technical Note.
- William, s., Foley, C. I., 1978. Steady-state Multi-ion Disturbed D-region Model, Hanscom AFB, Mass.: Aeronomy Division, Air Force Geophysics Laboratory, USA.
- Woods, T. N., Tobiska, W. K., Rottman, G. J., Worden, J. R., Dec. 2000. Improved solar Lyman α irradiance modeling from 1947 through 1999 based on UARS observations. *J. Geophys. Res.* 105, 27195-27216.

Table 1: Wait's parameters and electron densities at altitudes $h = 70, 75$ and 80 km obtained by data from [Han et al. \(2011\)](#), [McRae and Thomson \(2000\)](#) and [Friedrich and Torkar \(2001\)](#) for solar zenith angles related to locations of the transmitter (A) and receiver (B) in considered cases. $\Delta\%$ show deviations of these values from their mean values.

DATA SOURCE	CASE		H'	β	N		
					70 km	75 km	80 km
Han et al. (2011)	I	A	73.2 km	0.385 km^{-1}	$1.15 \cdot 10^8 \text{ m}^{-3}$	$3.72 \cdot 10^8 \text{ m}^{-3}$	$1.20 \cdot 10^9 \text{ m}^{-3}$
		B	73.1 km	0.385 km^{-1}	$1.19 \cdot 10^8 \text{ m}^{-3}$	$3.87 \cdot 10^8 \text{ m}^{-3}$	$1.25 \cdot 10^9 \text{ m}^{-3}$
		$\Delta\%$	0.07 %	0.00 %	1.92 %	1.92 %	1.92 %
	II	A	74.8 km	0.381 km^{-1}	$6.32 \cdot 10^7 \text{ m}^{-3}$	$2.01 \cdot 10^8 \text{ m}^{-3}$	$6.37 \cdot 10^8 \text{ m}^{-3}$
		B	75.2 km	0.377 km^{-1}	$5.54 \cdot 10^7 \text{ m}^{-3}$	$1.72 \cdot 10^8 \text{ m}^{-3}$	$5.37 \cdot 10^8 \text{ m}^{-3}$
		$\Delta\%$	0.27 %	0.53 %	6.57 %	7.57 %	8.56 %
	III	A	73.9 km	0.374 km^{-1}	$9.16 \cdot 10^7 \text{ m}^{-3}$	$2.81 \cdot 10^8 \text{ m}^{-3}$	$8.60 \cdot 10^8 \text{ m}^{-3}$
		B	74.1 km	0.378 km^{-1}	$8.36 \cdot 10^7 \text{ m}^{-3}$	$2.61 \cdot 10^8 \text{ m}^{-3}$	$8.17 \cdot 10^8 \text{ m}^{-3}$
		$\Delta\%$	0.14 %	0.53 %	4.56 %	3.56 %	2.56 %
McRae and Thomson (2000)	I	A	71.6 km	0.377 km^{-1}	$2.15 \cdot 10^8 \text{ m}^{-3}$	$6.70 \cdot 10^8 \text{ m}^{-3}$	$2.09 \cdot 10^9 \text{ m}^{-3}$
		B	71.6 km	0.376 km^{-1}	$2.16 \cdot 10^8 \text{ m}^{-3}$	$6.68 \cdot 10^8 \text{ m}^{-3}$	$2.07 \cdot 10^9 \text{ m}^{-3}$
		$\Delta\%$	0 %	0.13 %	0.08 %	0.17 %	0.42 %
	II	A	74.1 km	0.324 km^{-1}	$1.04 \cdot 10^8 \text{ m}^{-3}$	$2.49 \cdot 10^8 \text{ m}^{-3}$	$5.94 \cdot 10^8 \text{ m}^{-3}$
		B	74.8 km	0.311 km^{-1}	$8.85 \cdot 10^7 \text{ m}^{-3}$	$1.98 \cdot 10^8 \text{ m}^{-3}$	$4.43 \cdot 10^8 \text{ m}^{-3}$
		$\Delta\%$	0.47 %	2.05 %	8.20 %	11.42 %	14.61 %
	III	A	72.7 km	0.355 km^{-1}	$1.51 \cdot 10^8 \text{ m}^{-3}$	$4.21 \cdot 10^8 \text{ m}^{-3}$	$1.17 \cdot 10^9 \text{ m}^{-3}$
		B	72.9 km	0.351 km^{-1}	$1.42 \cdot 10^8 \text{ m}^{-3}$	$3.89 \cdot 10^8 \text{ m}^{-3}$	$1.06 \cdot 10^9 \text{ m}^{-3}$
		$\Delta\%$	0.14 %	0.57 %	2.97 %	3.97 %	4.97 %
Friedrich and Torkar (2001)	I	A	71.0 km	0.263 km^{-1}	$3.03 \cdot 10^8 \text{ m}^{-3}$	$5.33 \cdot 10^8 \text{ m}^{-3}$	$9.37 \cdot 10^8 \text{ m}^{-3}$
		B	71.0 km	0.263 km^{-1}	$3.03 \cdot 10^8 \text{ m}^{-3}$	$5.33 \cdot 10^8 \text{ m}^{-3}$	$9.37 \cdot 10^8 \text{ m}^{-3}$
		$\Delta\%$	0 %	0 %	0 %	0 %	0 %
	II	A	75.2 km	0.226 km^{-1}	$1.22 \cdot 10^8 \text{ m}^{-3}$	$1.78 \cdot 10^8 \text{ m}^{-3}$	$2.60 \cdot 10^8 \text{ m}^{-3}$
		B	77 km	0.217 km^{-1}	$8.62 \cdot 10^7 \text{ m}^{-3}$	$1.21 \cdot 10^8 \text{ m}^{-3}$	$1.68 \cdot 10^8 \text{ m}^{-3}$
		$\Delta\%$	1.18 %	2.03 %	17.02 %	19.20 %	21.36 %
	III	A	72.4 km	0.245 km^{-1}	$2.19 \cdot 10^8 \text{ m}^{-3}$	$3.52 \cdot 10^8 \text{ m}^{-3}$	$5.66 \cdot 10^8 \text{ m}^{-3}$
		B	72.9 km	0.241 km^{-1}	$1.96 \cdot 10^8 \text{ m}^{-3}$	$3.09 \cdot 10^8 \text{ m}^{-3}$	$4.86 \cdot 10^8 \text{ m}^{-3}$
		$\Delta\%$	0.34 %	0.82 %	5.54 %	6.54 %	7.53 %

Table 2: Error factors EF for given method for implementation electron density values obtained by our procedure versus those calculated from data presented in Han et al. (2011), McRae and Thomson (2000) and Friedrich and Torkar (2001) for solar zenith angles related to the transmitter (A) and receiver (B) locations in considered cases and given in Eq. 10.

DATA SOURCE	CASE		EF		
			70 km	75 km	80 km
Han et al. (2011)	I	A	1.01	1.54	2.35
		B	0.97	1.48	2.27
	II	A	0.53	0.80	1.20
		B	0.47	0.69	1.01
	III	A	0.77	1.12	1.62
		B	0.70	1.04	1.54
McRae and Thomson (2000)	I	A	1.82	2.67	3.92
		B	1.82	2.66	3.89
	II	A	0.88	1.00	1.12
		B	0.75	0.79	0.83
	III	A	1.27	1.68	2.21
		B	1.20	1.55	2.00
Friedrich and Torkar (2001)	I	A	2.55	2.12	1.76
		B	2.55	2.12	1.76
	II	A	1.03	0.71	0.49
		B	0.73	0.48	0.32
	III	A	1.84	1.40	1.06
		B	1.65	1.23	0.91